Detailed study of the nuclear dependence of the EMC effect and short-range correlations

J. Arrington, A. Daniel, D. B. Day, N. Fomin, D. Gaskell, and P. Solvignon

A detailed study of the nuclear dependence of the EMC effect and short-range correlations

J. Arrington,[1] A. Daniel,[2,3] D. B. Day,[3] N. Fomin,[4] D. Gaskell,[5] and P. Solvignon[5]

[1]*Physics Division, Argonne National Laboratory, Argonne, IL, 60439, USA*
[2]*Ohio University, Athens, OH, 45701, USA*
[3]*University of Virginia, Charlottesville, VA, 22904, USA*
[4]*Los Alamos National Laboratory, Los Alamos, NM, 87545, USA*
[5]*Thomas Jefferson National Accelerator Facility, Newport News, VA, 23606, USA*

Background: The density of the nucleus has been important in explaining the nuclear dependence of the quark distributions, also known as the EMC effect, as well as the presence of high-momentum nucleons arising from short-range correlations (SRCs). Recent measurements of both of these effects on light nuclei have shown a clear deviation from simple density-dependent models.

Purpose: A better understanding of the nuclear quark distributions and short-range correlations requires a careful examination of the experimental data on these effects to constrain models that attempt to describe these phenomena.

Methods: We present a detailed analysis of the nuclear dependence of the EMC effect and the contribution of SRCs in nuclei, comparing to predictions and simple scaling models based on different pictures of the underlying physics. We also make a direct, quantitative comparison of the two effects to further examine the connection between these two observables related to nuclear structure.

Results: We find that, with the inclusion of the new data on light nuclei, neither of these observables can be well explained by common assumptions for the nuclear dependence. The anomalous behavior of both effects in light nuclei is consistent with the idea that the EMC effect is driven by either the presence of high-density configurations in nuclei or the large virtuality of the high-momentum nucleons associated with these configurations.

Conclusions: The unexpected nuclear dependence in the measurements of the EMC effect and SRC contributions appear to suggest that the local environment of the struck nucleon is the most relevant quantity for explaining these results. The common behavior suggests a connection between the two seemingly disparate phenomena, but the data do not yet allow for a clear preference between models which aim to explain this connection.

I. INTRODUCTION

The nucleus is a system of strongly-interacting protons and neutrons. The characteristic scale for the nucleon momentum is the Fermi momentum, $k_F \approx 200$–270 MeV/c, a consequence of the interaction of the nucleon with the mean field of the nucleus. The strongly repulsive nature of the nucleon-nucleon (NN) interaction at short distances prevents two nucleons from coming very close together and this loss of configuration space demands the existence of high-momentum components in the nuclear ground state wave function. These can not be described in the context of mean field models and are commonly called short-range correlations (SRCs). Inelastic electron scattering was suggested long ago [1] to be a source of qualitative information on SRCs, yet they remain one of the least-well characterized aspects of the structure of stable nuclei.

Knockout reactions studied in inclusive and exclusive electron scattering [2–9] have isolated SRCs by probing the high-momentum tail of the nuclear momentum distribution. The tail is assumed to be the result of short-range hard interactions between nucleons [2, 10, 11], allowing a study of short-distance structure via reactions with high-momentum nucleons. The strength of SRCs in the nucleus has long been assumed to scale with nuclear density [2, 5, 6, 10, 12], a proxy for the probability of two nucleons interacting at short distances.

Typical parametrizations of the repulsive core of the NN interaction [13–15] show a sharp rise in the potential well below 1 fm. Because the nucleon has an RMS radius of roughly 0.85 fm [16], nucleon wave-functions can have significant overlap. In heavy nuclei, the typical inter-nucleon separation is 1.6 fm, suggesting that the nucleons have some overlap most of the time, and this short-range interaction may cause a modification of the structure of the nucleon. There is a long history of searches for this kind of "medium modification" of nucleon structure through measurements of the in-medium nucleon form factors [17–19] or modification of the quasielastic response in nuclei [20–24]. Overlap of the nucleon wave-functions may also allow for direct quark exchange, providing a new mechanism for modifying quark momentum distributions in the nucleus and one may expect them, like SRCs, to have a dependence on the average nuclear density.

The modification of the quark momentum distributions was first observed by the EMC collaboration [25] and is commonly referred to as the EMC effect. It was discovered that the per nucleon cross section in deep in-

elastic scattering (DIS) was different for iron and the deuteron. Because the binding energy of nuclei is extremely small compared to the energy scales in DIS, the early assumption was that the parton distribution functions (pdfs) of the nucleus would be a simple sum of the proton and neutron pdfs, except at the largest values of the quark momentum fraction (Bjorken-x) where the Fermi motion of the nucleus becomes important. Since the DIS cross sections depend on the quark distributions, the difference in the measured cross sections for iron and the deuteron indicated a suppression of quark pdfs in nuclei for $0.3 < x < 0.7$, and the size of this effect was seen to scale with the nuclear density.

Thus, the nuclear density has often been taken as the underlying cause of both the A dependence of the nuclear pdfs and the presence of short-distance configurations which give rise to high-momentum nucleons. Because of this, it is natural to assume that the behavior of both the EMC effect and the presence of SRCs will be closely connected. The relationship between these two effects was recently quantified [26], via a linear correlation between the SRCs in the tail of the nucleon momentum distribution and the size of the EMC effect.

While the EMC measurements performed in the '80s and '90s were well described by a density-dependent fit [27], the weak A dependence for these nuclei could be equally well described in other approaches that have been proposed [28, 29]. For example, some works have explained the effect in terms of the average virtuality ($\nu = p^2 - m_N^2$) of the nucleons [10, 30, 31], connecting it more closely to the momentum distributions. Given the limited precision of the EMC effect measurements and the fact that it grows smoothly but slowly for heavy nuclei, it is difficult to make a clear determination of which approach best describes its A dependence.

Recent measurements on light nuclei [9, 32] have observed a clear breakdown of the density-dependent picture for both the nuclear modification of quark pdfs and the strength of short-range correlations in nuclei, while still preserving the linear correlation between the two [33]. In this work, we provide a detailed analysis of the nuclear dependence of these two quantities, focusing on comparisons to model-inspired assumptions. We also perform an extended version of the analysis presented in Refs. [26, 33], aimed at testing the possible explanations for the correlation. For both the analysis of the A dependence and the direct comparison of the EMC and SRC data, we examine in more detail the meaning of the observables associated with these effects. As the underlying dynamics behind the examination of the direct correlation differ, additional corrections may be required when comparing the observables that are typically associated with the EMC effect or the presence of SRCs.

II. NUCLEAR DEPENDENCE OF THE EMC EFFECT

Deep inelastic scattering provides access to the quark distributions in nuclei via measurements of inclusive cross sections. This cross section for electron or muon scattering from a nucleus can be written as

$$\frac{d\sigma}{dxdQ^2} = \frac{4\pi\alpha^2 E'^2}{xQ^4}\frac{E'}{E}\left[F_2\cos^2\frac{\theta}{2} + \frac{2\nu}{M}F_1\sin^2\frac{\theta}{2}\right], \quad (1)$$

where F_1 and F_2 depend on x and Q^2. In the parton model, information about the quark distribution functions is encoded in the F_1 and F_2 structure functions. In the Bjorken limit (Q^2, $\nu \to \infty$, fixed $\frac{\nu}{Q^2}$), the structure functions become independent of Q^2,

$$F_1(x) = \frac{1}{2}\sum_q e_q^2 q(x), \quad F_2(x) = 2xF_1, \quad (2)$$

where $q(x)$ is the quark distribution function and e_q is the quark charge for a given flavor (u, d, s).

The per-nucleon ratio of the F_2 structure functions between an isoscalar nucleus and the deuteron is then a direct measure of the modification of quark distributions in nuclei. Experimentally, this ratio is defined as $R_{EMC} = (F_2^A/A)/(F_2^D/2)$. The deuteron structure function in the denominator is taken to approximate the sum of free proton and neutron structure functions. In almost all measurements of the EMC effect, an additional assumption is made that the ratio of longitudinal to transverse cross sections, $R = \sigma_L/\sigma_T$, is A-independent such that the unseparated ratio of cross sections corresponds directly to the F_2 ratio, i.e., $\sigma_A/\sigma_D = F_2^A/F_2^D$. For non-isoscalar nuclei an additional correction is typically applied to account for the difference in DIS cross sections between protons and neutrons.

Figure 1 shows a measurement of the EMC ratio for carbon from Ref. [32]. The region from $x = 0.3$ to 0.7 shows the depletion in the cross section ratio characteristic of all nuclei. The increase of the cross section ratio at large x is attributed to the greater Fermi momentum in the heavy nucleus as compared to the deuteron. The shape of the EMC ratio appears to be universal, independent of nucleus, while the magnitude of the suppression generally increases with A.

The origin of the EMC effect has been a topic of intense theoretical discussion since its original observation. There have been many explanations proposed, and these can be broadly broken down into two categories. The first includes only "traditional" nuclear physics effects, using convolution models with binding effects, detailed models of the nucleon momentum distribution, or pion-exchange contributions. The other category invokes more exotic explanations such as re-scaling of quark distributions in the nuclear environment, contributions of six or nine quark bags, or modification of the internal structure of the nucleons such as "nucleon swelling" or suppression
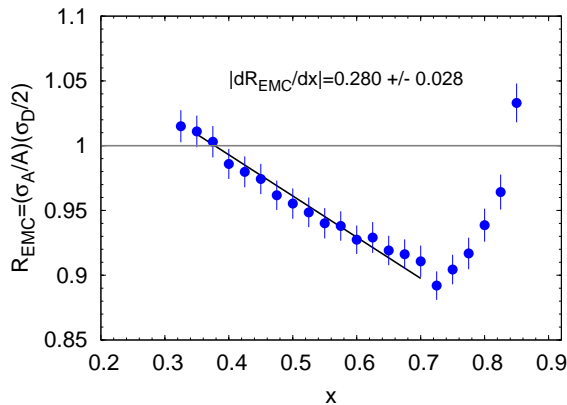
FIG. 1: (color online) EMC ratio, $(\sigma_A/A)/(\sigma_D/2)$, for carbon [32]. Solid line is a linear fit for $0.35 < x < 0.7$.

of point-like nucleon configurations. Several reviews give an overview of models of the EMC effect [28, 29, 34].

Because the observed suppression of the F_2 structure function between $0.3 < x < 0.7$ is relatively straightforward to reproduce in a variety of approaches, it is difficult to evaluate the different models without also carefully examining the A dependence. Direct comparisons to calculations are limited by the fact that many calculations are made for nuclear matter, and extrapolated to finite nuclei by assuming some simple scaling with A or nuclear density. Others use more realistic nuclear structure input [35–37], but often do not include light nuclei. So rather than comparing directly to calculations of the EMC effect, we will examine its nuclear dependence, comparing the data to different parameters assumed to drive the modification of the nuclear pdfs.

In our examination of the A dependence, we use the data from SLAC E139 [27] and the recent data on light nuclei from Jefferson Lab E03-103 [32]. SLAC E139 sampled a range of nuclei from $A = 4$ to 197, allowing a large lever arm for studying the nuclear dependence. Jefferson Lab experiment E03-103 adds ^{3}He and additional precise data on ^{4}He, ^{9}Be, and ^{12}C. While the JLab data is at somewhat lower Q^2 values than the SLAC data, it has been shown that the target ratios in this Q^2 range have very little deviation from the DIS limit, even for W^2 values below 4 GeV^2 [32, 38, 39]. The E03-103 data that go into extracting the EMC slope examined in this work are all very near or above W^2=4 GeV^2.

We use the definition of the "size" of the EMC effect as introduced in [32], i.e., $|dR_{EMC}/dx|$, the value of the slope of a linear fit to the cross-section ratio for $0.35 < x < 0.7$. These limits were chosen to give a range of high precision data whose behavior was linear, but the extracted slope is not very sensitive to small changes in the x region chosen. This definition reduces the sensitivity to normalization errors, which would otherwise be significant if one were to assess the nuclear dependence at a fixed value of x, especially for light nuclei. The impact of normalization uncertainties for the deuteron measure-

ments (common to all ratios in a given experiment) is also reduced in this approach. This procedure makes use of the fact that the EMC effect has a universal shape for $x > 0.3$, exhibited by all experimental data.

Table I lists the EMC slopes extracted from the two data sets described above. We do not include data from earlier measurements due to their relatively poor precision and/or limited x-coverage.

TABLE I: Combined EMC results from JLab E03-103 [32] and SLAC E139 [27] (averaged over Q^2). For JLab data, $|dR_{EMC}/dx|$ was extracted in the $0.35 \leq x \leq 0.7$ range. SLAC data, whose binning was different, were fit over $0.36 \leq x \leq 0.68$. For both cases, statistical and point-to-point systematic uncertainties were applied to each x-bin and the normalization uncertainties (including the 1% normalization uncertainty on deuterium common to all ratios for the SLAC data) were applied to the extracted slope.

A	JLab	SLAC	Combined
^{3}He	0.070±0.028	–	0.070±0.028
^{4}He	0.198±0.027	0.191±0.061	0.197±0.025
Be	0.271±0.030	0.208±0.038	0.247±0.023
C	0.280±0.029	0.318±0.041	0.292±0.023
Al	–	0.325±0.034	0.325±0.034
^{40}Ca	–	0.350±0.047	0.350±0.047
Fe	–	0.388±0.032	0.388±0.033
Ag	–	0.496±0.051	0.496±0.052
Au	–	0.409±0.039	0.409±0.040

When considering the nuclear dependence of the EMC effect, it is important to be aware of corrections which depend on A or Z, such as Coulomb distortion [40]. The influence of the Coulomb field of the nucleus on the incident or scattered lepton is a higher order QED effect, but is not typically included in the radiative corrections procedures. In addition, the size of EMC effect is taken directly from the cross section ratio instead of the structure function ratio, thus assuming no nuclear dependence in $R = \frac{\sigma_L}{\sigma_T}$. Coulomb distortions introduce kinematic corrections and consequently have a direct effect on the extraction of R. An indication of nuclear dependence in R was observed recently [41] after applying Coulomb corrections to SLAC E139 and E140 [42] data. Coulomb distortion was accounted for in the JLab data, but not the SLAC data, where it is estimated to be negligible for nuclei lighter than ^{12}C and at most a 2% effect on the ^{197}Au EMC slope. These changes do not significantly affect the nuclear dependencies studied below.

The JLab and SLAC data also used different prescriptions to correct non-isoscalar nuclei. In the case of SLAC data, a simple, x-dependent parametrization was employed based on high Q^2 data for F_2^D/F_2^p. A more sophisticated correction was applied to the JLab data [32], using a smeared ratio of free proton and neutron cross sections [43]. Reanalysis of the SLAC data using the updated isoscalar corrections yields slightly larger EMC slopes for the very heavy nuclei, but does not impact the overall conclusions of this analysis. A detailed compari-

son of these effects for both the SLAC data and the heavy target data from JLab E03-103 is in progress [44, 45].

Early calculations of the EMC effect included only the impact of Fermi motion and were unable to give a significant suppression at large x. One can go beyond simple smearing by including the effect of the binding energy of the nucleus. However, the impact of the average nuclear binding is small and peaks $A = 56$, while the EMC effect continues to grow in heavier nuclei. Thus, the binding energy per nucleon, E_A/A, cannot explain the full modification of the nuclear pdfs [46].
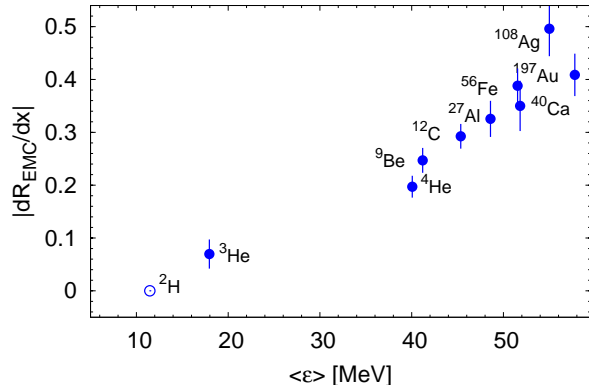

FIG. 2: (color online) Magnitude of the EMC effect, $|dR_{EMC}/dx|$, vs. the average nucleon separation energy. The empty circle indicates the known (zero) deuteron EMC slope.

While the nuclear binding energy is insufficient to explain the EMC effect, high-energy electron scattering involves a near instantaneous scattering and averages over all nucleons in the target. This suggests that the average separation energy may be the more relevant quantity in evaluating the effect of binding. The heart of the binding model describes nucleons bound in a nucleus with some non–zero three-momentum, and as a consequence of the nuclear binding, an energy modified from its usual on–shell value, i.e., $E_N \neq \sqrt{p_N^2 + m_N^2}$. The bound nucleon has a removal or separation energy ϵ, with its total energy given by $E_N = m_N + \epsilon$ (ignoring the kinetic energy of the recoiling nucleus). In practice the average separation energy is often determined using the Koltun sum rule [47],

$$\langle\epsilon\rangle + \frac{\langle p^2\rangle}{2m_N} = 2\frac{E_A}{A}, \tag{3}$$

where p is the nucleon three-momentum and E_A/A is the binding energy per nucleon. An alternate formulation of the above rule was by proposed in Ref. [48], incorporating a recoil factor, but is not used in the analysis presented here. The modification of the nucleon energy results in a value of $x = Q^2/2p_N \cdot q$ shifted by $\approx \langle\epsilon\rangle/m_N$. In this context, the depletion of the cross section for $A > 2$ in DIS is associated with off-shell nucleons and binding produces a simple rescaling of the relevant kinematic variable (x)

and does not imply an inherent modification of the nucleon structure in the nucleus. Refs. [28, 49] gives excellent overviews of early calculations of the EMC effect in the binding approach. This approach was relatively successful in reproducing the shape of the EMC effect at large x [35, 36, 50], although calculations including only this effect consistently underpredict the observed EMC effect.

Figure 2 shows the extracted EMC ratio as a function of the average nucleon separation energy, $\langle\epsilon\rangle$ from [51], which provides the most complete set of nuclei. In this figure, the separation energy was calculated from spectral functions used and described in [36, 52]; they include contributions from both mean–field and correlated (high-momentum) components of the nuclear wave function. While the separation energy is an inherently model–dependent quantity, we have investigated alternate definitions of the separation energy based on the Koltun sum rule as given in Eq. 3 and found that the typical agreement is usually better than 5 MeV. However, some calculations use modified estimates of $\langle\epsilon\rangle$, which can yield larger disagreements.

Qualitatively, the size of the EMC effect correlates very well with the average separation energy, as was also observed in another recent analysis [53], using a slightly different measure of the EMC effect and modified calculation of the mean separation energy. However, while the correlation with the EMC effect is good, detailed calculations based on the binding associated with the mean separation energy [35, 36] yield an effect that explains only part of the observed EMC effect. In addition, nuclear binding models have failed to gain traction in the past, usually due to the omission of the so-called "flux factor" (incorrect treatment of wave-function normalization) [50], exclusion of pions [30], and failure to describe the Drell-Yan data [54]. It thus seems unlikely that the modification of the nucleon pdfs in the nucleus can be explained by binding effects alone, and aspects of medium modification must be included [30, 46, 52, 55].

The E139 analysis [27] examined the nuclear dependence of the EMC effect in terms of an ad-hoc logarithmic A-dependence and the average nuclear density. In panel (a) of Fig. 3 we show the A dependence. While it is possible to construct a good linear fit for either light or heavy nuclei, no linear correlation exists for the whole data set.

Exact nuclear matter calculations [56] can be applied to finite nuclei within the local density approximation (LDA)[12, 57]. This provides an estimate of the A dependence for effects that depend on the nuclear density and is based on general characteristics of the nuclear density distributions. For $A > 12$, the nuclear density distribution $\rho(r)$ has a common shape and has been found to be relatively constant in the nuclear interior. Contributions to the lepton scattering cross section from this portion of the nucleus should then scale with A. The nuclear surface is also characterized by a nearly universal shape, $\rho(r-R)$, where R is the half-density radius $R = r_\circ A^{\frac{1}{3}}$, such that
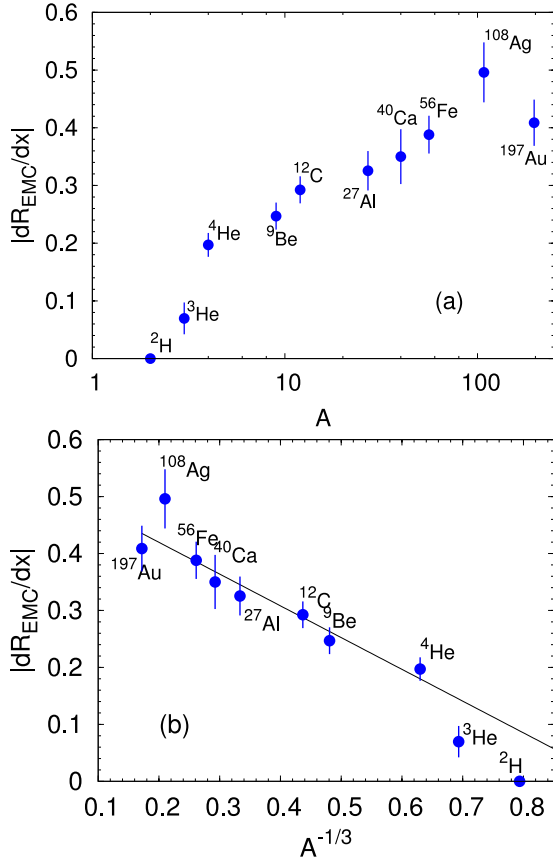
FIG. 3: (color online) Magnitude of the EMC effect vs. A (top) and $A^{-1/3}$ (bottom). The bottom plot includes a linear fit for $A \geq 12$.

contributions from the surface grow as R^2, or $A^{2/3}$. It then follows that the cross section per nucleon (dividing the separate contributions by A) should be constant with a small deviation that scales with $A^{-1/3}$, which is due to the reduced density of the surface region. For small-A nuclei the nuclear response is dominated by surface effects while for large-A nuclei the nuclear response is dominated by the constant density region. It has been argued that the response function (per nucleon) for nuclear matter can be extrapolated as a linear function of $A^{-1/3}$ to $A^{-1/3} = 0$ in the deep inelastic scattering region [57].

In panel (b) of Figure 3 the extracted EMC slope is plotted versus $A^{-1/3}$. Somewhat surprisingly, this yields one of the better correlations with the data, even for ^{12}C, ^{9}Be and ^{4}He. This is not expected, since the prediction of the $A^{-1/3}$ behavior is based on the assumption of an A-independent "surface" density distribution and a scaling with A of the volume/surface ratio. The assumption that the shape of the "surface" density is universal is certainly not valid for $A \leq 12$, and it is not clear that the concept of dividing the nucleus into a surface region and a high-density core is at all applicable to ^{3}He or ^{4}He.

The LDA predicts a simple A dependence based on the assumption that the EMC effect scales with den-
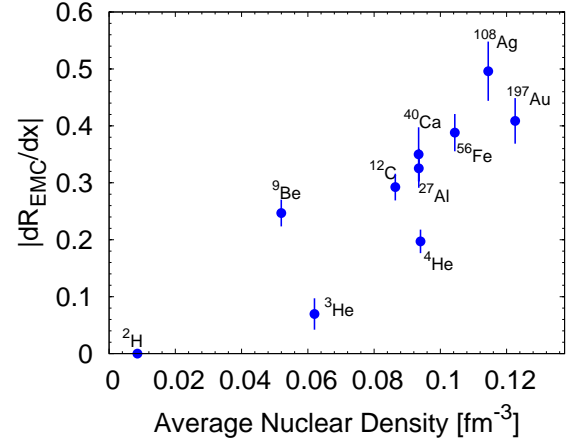

FIG. 4: (color online) Magnitude of the EMC effect vs. average nuclear density.

sity. Since this is not expected to work for light nuclei, one can evaluate the idea of a density-dependent EMC effect more directly by looking at the average nuclear density based on calculations or electron-scattering measurements of the nuclear mass (or charge) density. This dependence is shown in Figure 4. For light nuclei ($A \leq 12$), the average density is evaluated using density distributions extracted within Green's Function Monte Carlo (GFMC) calculations [58, 59], while for heavier nuclei it is derived from electron scattering extractions of the charge density [60]. This is in contrast to Ref. [27], in which the average density was calculated assuming a uniform sphere with radius equal to the RMS charge radius of the relevant nucleus, although for $A \geq 12$, this yields the same qualitative behavior as is seen in Fig. 4.
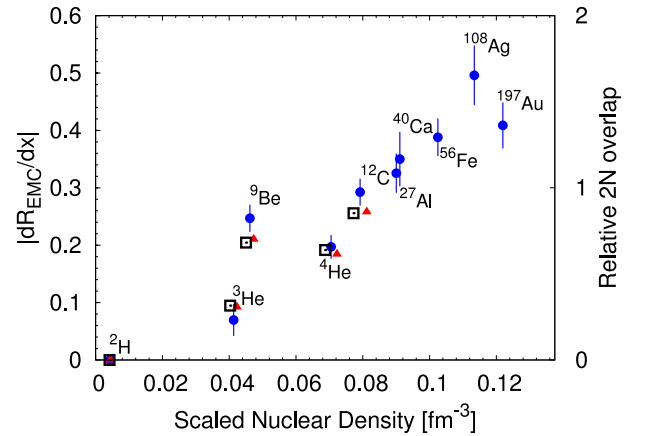

FIG. 5: (color online) Magnitude of the EMC effect (solid circles) vs. scaled nuclear density. The solid triangles and hollow squares show the calculated average 2N overlap from Eq. 5 minus the deuteron value, i.e. $\langle O_N \rangle_A - \langle O_N \rangle_D$ (RHS scale: See text for details). Overlap points are offset on the x-axis for clarity.

The relationship between EMC slope and density is improved when taking the scaled nuclear density, which

includes an additional correction factor of $(A-1)/A$, meant to account for the excess nuclear density seen by the struck nucleon. This is seen in Fig. 5, where the EMC effect grows approximately linearly with scaled density, with the exception of ^{9}Be. This was explained in Ref. [32] as being a result of the cluster–like structure of ^{9}Be, whose wave function includes a sizable component in which the nucleus can be thought of as two α clusters associated with a single neutron [61–63]. If the EMC effect is governed by the local density, rather than the average nuclear density, then it is not unreasonable that the size of the effect in ^{9}Be would be similar in magnitude to that in ^{4}He.

As mentioned earlier, nucleon wave-functions can have a significant amount of overlap in the nucleus before the nucleons come close enough to respond to the repulsive core. If we can quantify this overlap, it could provide a reasonable measure of the local density. We estimate this is by taking the 2-body density distributions from GFMC calculations [58, 59] which provide the distribution of the relative nucleon separation between pp, np, and nn configurations. If we integrate the normalized $\rho_2^{pp}(r)$ up to $r = 1.7$ fm, we find the probability that a proton is within 1.7 fm (twice the RMS radius of a nucleon) of another proton. Thus, we define a measure of the relative pair overlap between nucleons by taking

$$O_{NN} = \int_0^\infty W(r)\rho_2^{NN}(r)d^3r \qquad (4)$$

where $W(r)$ is a cutoff function used to evaluate the contribution at short distances. If $W(r)$ is a step function that cuts off at $r = R_0$, then O_{pn} represents the average probability that a given pn pair has a separation of R_0 or less. A proton, then, has an average overlap parameter $O_p = (Z-1)O_{pp} + NO_{pn}$, which for a step function with $R_0 \to \infty$ yields $(A-1)$, the total number of neighbor nucleons for the studied proton. To obtain the effective 2N overlap for a given reaction, we take a cross section weighted average of O_p and O_n:

$$\langle O_N \rangle = (Z\sigma_p O_p + N\sigma_n O_n)/(Z\sigma_p + N\sigma_n). \qquad (5)$$

We show the relative 2N overlap for two calculations in Fig. 5, subtracting the result for the deuteron, i.e. $\langle O_N \rangle_A - \langle O_N \rangle_D$. The solid triangles are for a step function with $R_0 = 1.7$ fm and $\sigma_n/\sigma_p = 0.5$, although the result is very insensitive to the exact value of σ_n/σ_p. Because the amount of overlap between nucleons decreases with the separation, $W(r)$ can be chosen to enhance the effect when the nucleons are extremely close together. The hollow squares are the result when we take $W(r)$ to be a gaussian centered at $r = 0$ with a width of 1 fm. An overall normalization factor is applied to compare to the A dependence of the EMC slopes. Both of these simple calculations of overlap yield a good qualitative reproduction of the behavior for light nuclei and one which is not very sensitive to the choice of the cutoff function or the exact scale of the cutoff parameter.

For all of the light nuclei, an average overlap parameter can be obtained from the *ab initio* GFMC calculations. This provides realistic input of the distribution of nucleons in these nuclei, although the quantitative evaluation of the overlap parameter does depend on the somewhat arbitrary choice of the cutoff function in Eq. 4. One could use measurements of short-range correlations in nuclei as an observable which is also sensitive to the relative contribution from short-distance configurations in nuclei. This is a possible interpretation of the correlation observed between SRC measurements and the EMC effect, and we will present this in detail after examining the A dependence of the short-range correlation measurements.

To definitively test the notion that the EMC effect depends on "local density", additional data on light nuclei, especially those with significant cluster structure, are required. Such studies are planned as part of the program after the Jefferson Lab 12 GeV Upgrade [64].

III. NUCLEAR DEPENDENCE OF SHORT RANGE CORRELATIONS

Much as DIS isolates scattering from quasi-free quarks, quasielastic (QE) scattering isolates incoherent scattering from the protons and neutrons in the nucleus. This allows us to study the momentum distributions of the bound nucleons [65]. Inclusive electron scattering can be used to pick out contributions from high-momentum nucleons in SRCs by going to $x > 1$ kinematics [2, 11, 65].

In the QE regime, we can decompose the cross section into contributions from single-nucleon scattering (mean-field independent particle contributions) and scattering from 2-nucleon, 3-nucleon, etc correlations [2] via:

$$\sigma(x, Q^2) = \sum_{j=1}^A A\frac{1}{j}a_j(A)\sigma_j(x, Q^2) \qquad (6)$$

where $\sigma_j(x, Q^2) = 0$ at $x > j$ and the $a_j(A)$'s are proportional to the probabilities of finding a nucleon in a j–nucleon correlation. In the case of the electron–deuteron cross section, σ_2 will be dominated by contributions from 2N correlations for $x > 1.4$, where the nucleon momentum is well above k_F and the mean field contribution has died off. In this case, a_2 is closely related to the number of 2N correlations in the nucleus (per nucleon) relative to that of the deuteron. Hence Eq. 6 expresses the fact that in the region $j < x < j + 1$ the contribution of j–nucleon SRCs dominates. This result is in reasonable agreement with numerical calculations of the nuclear spectral functions [66, 67].

Equation (6) suggests scaling relations between scattering off the heavy nuclei and the deuteron:

$$\frac{\sigma_A(x, Q^2)/A}{\sigma_D(x, Q^2)/2} = a_2(A) \mid_{1.4 \lesssim x \leq 2} \qquad (7)$$

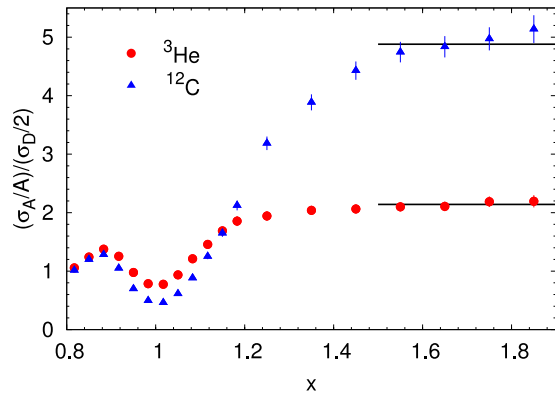The scaling of the cross section ratios has been established, first at SLAC [2] and at Jefferson Lab [5, 6, 9].

FIG. 6: (color online) Per nucleon cross section ratios for ^{3}He/^{2}H and ^{12}C/^{2}H measured at JLab [9] at $18°$. In the region dominated by 2N SRCs the ratios becomes independent of x. The dip around $x=1$ is the result of $A > 2$ nuclei having wider quasielastic peaks and the solid line indicates the region used to extract the ratio a_2.

The most recent experiment measured this scaling precisely in the 2N correlation region for a range of nuclei with selected data shown in Fig. 6.

In extracting the relative contributions of 2N SRCs in the inclusive cross section ratios at $x > 1$, it has typically been assumed that the electron is scattering from a pair of nucleons with large relative momentum but zero total momentum, such that the cross section for scattering from a neutron-proton pair in a nucleus is identical to the cross section for scattering from a deuteron. In this case, the elementary electron–nucleon cross sections as well as any off-shell effects cancel in taking the ratio. Final state interactions are also assumed to cancel in the cross section ratios [2, 11].

Earlier analyses [2, 5, 6] assumed that the SRCs would be isospin-independent, with equal probability for pp, np, and nn pairs to have hard interactions and generate high-momentum nucleons. This necessitated an "isoscalar correction" to account for the excess of nn (or pp) pairs in non-isoscalar nuclei as well as the difference between the $e-p$ and $e-n$ elastic cross sections. More recently, measurements of two-nucleon knockout showed that these correlations are dominated by np pairs [8, 68] due to the fact that the bulk of the high-momentum nucleons are generated via the tensor part of the N–N interaction rather than the short-range repulsive core [69, 70]. The most recent experiment [9] to precisely measure SRCs on a range of nuclei did not apply this isoscalar correction, and presented results for previous measurements with this correction removed.

The per nucleon cross section ratio at large x provides a direct measure of the contribution of high-momentum nucleons relative to the deuteron. However, this is not equal to the relative number of SRCs, since in $A > 2$ nuclei, the correlated pair experiences motion in the mean field created by the rest of the nucleons. The momentum distribution of the pair will be smeared out, which

will flatten the top of the QE peak, depleting the low-momentum part of the distribution, but enhancing the high-momentum tail. The effect is illustrated in Fig. 7 which shows the deuteron momentum distribution along with an estimate of the momentum distribution for an np pair in iron. The "smeared deuteron" curve is generated by taking the high-momentum part of the deuteron distribution and convolving it with a pair c.m. distribution to estimate the impact of the motion of the correlated pair in the nucleus. This is combined with a gaussian distribution whose width is chosen to reproduce a mean field calculation for iron [67], and whose magnitude is such that the total distribution is properly normalized.
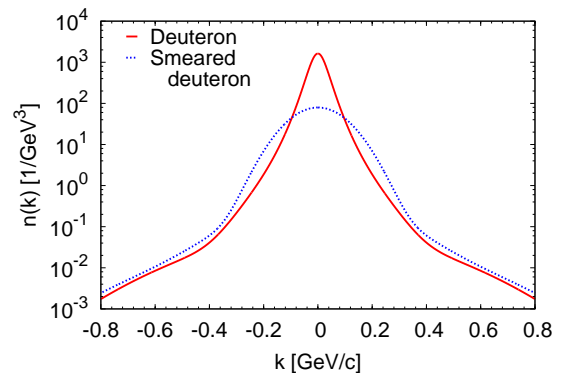

FIG. 7: (color online) Momentum distribution for the free deuteron and an np pair in iron, taken as the sum of a mean field (gaussian) contribution and the convolution of the high-momentum deuteron tail with the c.m. motion of the pair in iron.

A correction for this redistribution of strength was first applied in Ref. [9], where analyses of previous experiments were also updated. The correction procedure was based on the calculation of Ref. [67], where the deuteron momentum distribution was convolved with a parametrization of c.m. motion of the pair, which yielded a 20% enhancement in the high momentum tail for iron. This correction was applied to the other nuclei by assuming that the enhancement in the ratio, which scales with the c.m. momentum of the pair, was proportional to the Fermi motion of the nucleus.

We performed a similar convolution calculation for a variety of nuclei, and found a slightly larger correction, above 30% for iron. We also observed that the size of the effect depends on the momentum region examined, the details of the deuteron momentum distribution and the assumed c.m. momentum distribution. While the enhancement is relatively constant at large k, it does increase for very large momenta. This effect is at least partially responsible for the small rise of the SRC ratios for $x \to 2$.

Another recent attempt to estimate the role of c.m. motion [71] yielded significantly larger corrections, although it is not yet clear what explains this difference. In all of the above cases, the correction has only a very weak nu-

clear dependence, mostly yielding an overall scaling factor for the SRC ratios, without significant impact on the linear correlation between them and the EMC effect. We use the correction and uncertainty applied in Ref. [9], but it is clear that this is an issue requiring further study.

TABLE II: Existing measurements of SRC ratios, R_{2N}, all corrected for c.m. motion of the pair and excluding the isoscalar correction applied to earlier extractions. The second-to-last column combines all the measurements, and the last column shows the ratio a_2, obtained without applying the c.m. motion correction. SLAC and CLAS results do not have Coulomb corrections applied, which would raise the CLAS Fe ratio by ∼5%, and the SLAC Au data by ∼10% (correction is kinematic-dependent).

	E02-019	SLAC	CLAS	R_{2N}-ALL	a_2-ALL
^{3}He	1.93±0.10	1.8±0.3	–	1.92±0.09	2.13±0.04
^{4}He	3.02±0.17	2.8±0.4	2.80±0.28	2.94±0.14	3.57±0.09
Be	3.37±0.17	–	–	3.37±0.17	3.91±0.12
C	4.00±0.24	4.2±0.5	3.50±0.35	3.89±0.18	4.65±0.14
Al	–	4.4±0.6	–	4.40±0.60	5.30±0.60
Fe	–	4.3±0.8	3.90±0.37	3.97±0.34	4.75±0.29
Cu	4.33±0.28	–	–	4.33±0.28	5.21±0.20
Au	4.26±0.29	4.0±0.6	–	4.21±0.26	5.13±0.21

For the purposes of our analysis, we combine the results of the JLab Hall-C [9], Jlab Hall-B (CLAS) [6] and SLAC [2] measurements. The combined data set provides a large collection of nuclei to examine the A dependence of the extracted SRC contributions. Table II shows a_2, the raw A/D cross section ratio, as well as R_{2N}, where the c.m. motion correction has been applied. The meanings of the two quantities are subtly different. a_2 represents the relative strength of the high-momentum tail, i.e. the total contribution from high momentum nucleons relative to the deuteron. For iron, $R_{2N} \approx 4$, implying that a nucleon in iron is four times more likely to be part of an SRC than a nucleon in a deuteron, At the same time a_2 is ≈ 4.8, which means that there are almost five times as many high momentum nucleons in the tail of the distribution for iron as there are for the deuteron. This 20% enhancement comes about due to the c.m. motion of the correlated pair.

We use R_{2N} for the nuclear dependence tests, as we are examining the behavior of the number of SRC pairs relative to the deuteron. Since the c.m. correction factor applied to a_2 has very little A dependence, the nuclear dependence a_2 is very similar to that of R_{2N}.

Figure 8 shows R_{2N} as a function of $A^{-1/3}$, the behavior expected in the LDA [12, 57]. While R_{2N} is a relatively smooth function of $A^{-1/3}$, there is not a simple, linear relation suggesting a proportionality. As with the EMC effect, the prediction of scaling with $A^{-1/3}$ is an approximation which is not expected to be valid for very light nuclei.

For nuclei with similar forms for $\rho(r)$, we expect to see scaling of the SRCs, that is, denser nuclei are more likely to have short range configurations. Figure 9 shows
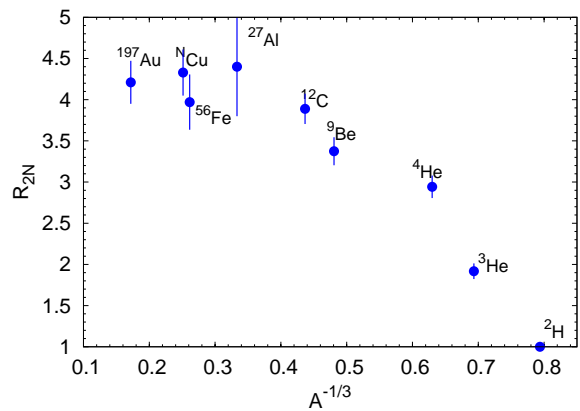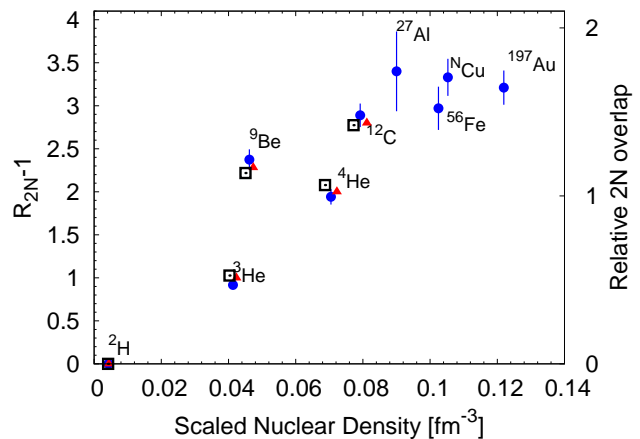

FIG. 8: (color online) R_{2N} versus $A^{-1/3}$.

FIG. 9: (color online) R_{2N} versus scaled nuclear density (solid circles). The solid triangles and hollow squares show the calculated 2N overlap minus the deuteron value (RHS scale) from Eq. 5. Points offset on the x-axis for clarity.

R_{2N} as a function of the scaled nuclear density, defined in the previous section. It is clear that the simple density-dependent model does not track the behavior of the light nuclei, whose large deviations are reminiscent of those shown by the EMC effect [32].

While there were few calculations for the nuclear dependence of the EMC effect that went beyond a simple scaling with A or density, there are more calculations for the A dependence of short-range correlations. The authors of Ref. [72] estimate the relative SRC contribution in a variety of nuclei based on the mean field densities of the nuclei. Ref. [73] estimates the high-momentum contributions based on the presence of deuteron-like pairs in the nucleus. In both of these approaches, they predict a stronger rise of the SRC contributions with A than is observed in the data. The latter result [73] displays a sensitivity to the c.m. motion correction [71], yielding an even sharper rise with A. An earlier work [74] estimated the probability for multi-quark ($6q$, $9q$,...) clusters in nuclei based on the probabilty of overlap of two or more nucleons within some critical separation, which should

also be closely related to the contribution of 2N and 3N-SRCs. They find that the probability for $6q$ configurations scales roughly with the density of the nucleus, with the exception of ^{4}He, where a much larger contribution is predicted. In the data, the SRC ratio in ^{9}Be is significantly larger than expected for a model which scales with density, and ^{4}He does not show the anomalously large contribution predicted by this calculation.

As with the analysis of the EMC effect, we also show the relative 2N overlap from Eq. 5 as a function of the scaled nuclear density in Figure 9. As before, the overlap for the deuteron has been subtracted for $A > 2$. The density dependence of SRCs is well reproduced by the overlap calculation, as they both reflect the abundance of short-distance configurations. This allows us to use SRC ratios as an experimental measure of overlap, extending the comparison with the EMC effect in Fig. 5 to $A > 12$. Such a comparison assumes a certain connection between SRCs and the EMC effect, which will be examined in detail in the next section, along with an alternate possibility.

IV. DETAILED COMPARISON OF SRC AND EMC RESULTS

As discussed in the introduction, there have been previous comparisons of the nuclear dependence of the size of the EMC effect and the contributions from SRCs in nuclei [26, 33]. Given the data available in the initial analysis, the correlation seen between the two effects could be explained by a common density- or A-dependent scaling. However, the new data on the EMC effect [32] and SRCs [9] rule out this simple explanation, while exhibiting almost identical trends versus both density and A, shown in Fig. 10. For the EMC effect, it was suggested that if the local environment of the struck nucleon drives the modification of the quark distributions, then the strong contribution of α-like clusters would make ^{9}Be behave like a much denser nucleus. The nearly identical behavior of ^{9}Be in the SRC extraction [9] supports this idea, as the SRC measurements directly probe the short-distance structure. Even with these new data and their unexpected but common trend, the linear relationship observed in [26] is still apparent [33]. This suggests that a careful re-examination of the linear correlation is in order to try to better understand its underlying cause.

First, we note that the initial comparison of the EMC effect and SRCs used extractions of the SRCs which included an isoscalar correction for nuclei with unequal numbers of protons and neutrons and did not apply corrections for c.m. motion of the correlated pair. It has been shown that SRCs are made-up of predominantly np pairs due to the tensor interaction [8, 69, 70], making the isoscalar correction unnecessary. The question of the c.m. motion correction is somewhat more complicated in the context of the direct comparison of the EMC and SRC results. Whether or not this correction should be
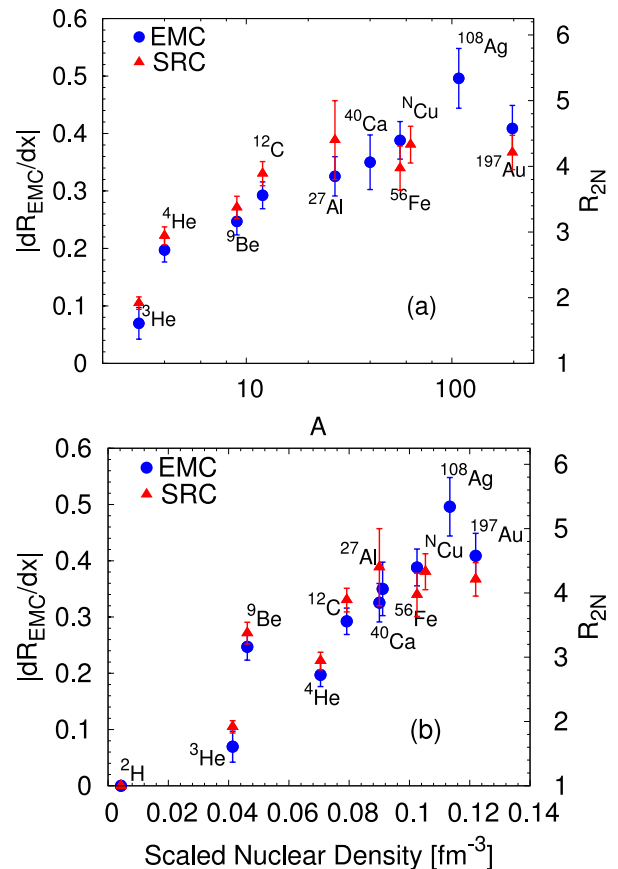

FIG. 10: (color online) Size of the EMC effect ($|dR_{EMC}/dx|$) as well as the relative measure of SRCs (R_{2N}) are shown as a function of A (top) and scaled nuclear density (bottom).

applied in this analysis depends on exactly what correlation is being examined, and so we focus now on the different explanations for this correlation.

The fact that ^{9}Be so obviously violates the density dependence for both effects in the same way suggests that an altered density dependence, such as "local density" (LD) may give us a good description of both effects. One should then compare the size of the EMC effect to R_{2N}, which represents the relative probability that a nucleon will be part of a very short-distance configuration (a deuteron-like SRC). For extremely small nucleon separations, the short-range repulsive core will yield hard interactions, and thus high momenta, for all NN pairs. However, the bulk of the SRCs observed are np pairs [8], generated by the longer-range tensor interaction. If nn, np, and pp pairs all have equal probability to form high local density configurations, we would expect that the EMC effect should scale with the number of possible NN pairs in the nucleus, $N_{tot} = A(A-1)/2$, while the SRC contribution is sensitive to only the possible np pairs, $N_{iso} = NZ$. For light nuclei, we test this assumption by examining the two-body density distributions [58, 59] for all NN pairs. Taking nuclei up to $A=12$, the np pairs have a larger probability to have small separation,

on average 10-20% more than for pp or nn pairs at separations below 1.7 fm. So while the assumption that all pairs contribute equally at short distances isn't exact, it's significantly better than assuming that only np pairs contribute. Thus, we scale the SRC ratio by a factor N_{tot}/N_{iso} to account for the difference in the pair counting for the EMC and SRC data, which is a simple first-order correction that neglects the possible impact of nuclear structure effects.
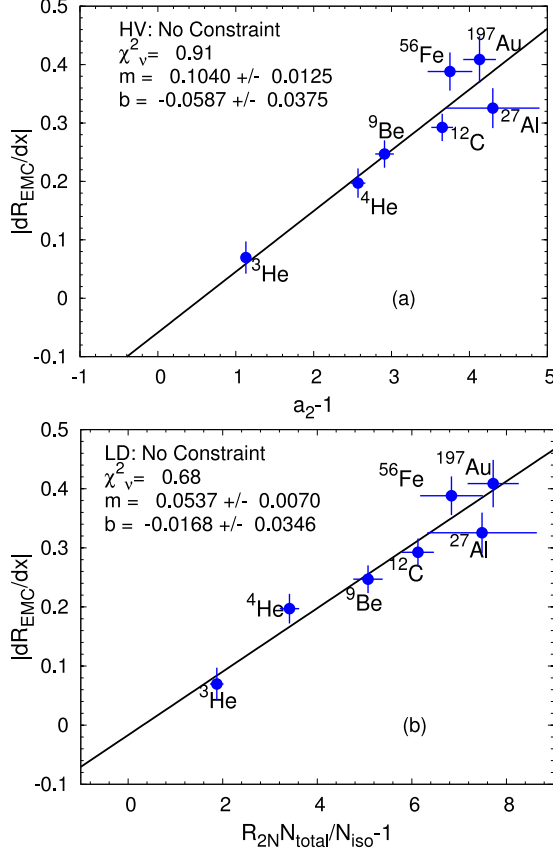

FIG. 11: (color online) Comparison of EMC slopes and SRC observables from world's data where both observables are available for the same nuclei. The top plot shows the EMC slope vs. a_2, testing the high virtuality interpretation. Analogously, the bottom plot shows the EMC slope vs. R_{2N} scaled by N_{tot}/N_{iso}, testing the local density interpretation (as discussed in the text) along with fits.

A different hypothesis to explain the linear relationship between the two effects was proposed by Weinstein et al [26], suggesting that the EMC effect is driven by the virtuality of the high-momentum nucleon [10, 31]. In this case, it is the relative probability for a nucleon to have high momentum ($> k_F$) that should drive the EMC effect, and thus the uncorrected a_2 SRC ratio is a more direct indicator of the underlying explanation. We will refer to this hypothesis as "high-virtuality" (HV).

We now make two comparisons to examine the relationship between the EMC effect and SRCs using these two different underlying assumptions. The data as well as

the linear fits for both approaches are shown in Fig. 11. A two-parameter linear fit is performed for both cases without any constraint for the deuteron. Thus, we can examine the fit to test both the linear correlation of the observables and the extrapolation to the expected deuteron value. The intercept of the fit is expected to be zero, since both the EMC effect and SRC contributions are taken relative to the deuteron.

Both approaches yield reasonable results, but we have to delve into the details to understand the impact of the small differences. While the LD fit has a better χ^2_ν value, the fractional errors of the points of the x-axis are larger due to the additional model-dependent uncertainties arising from the c.m. motion correction [9]. A 30% uncertainty was applied for this A-dependent correction, but any error in this correction is likely to have a smooth A dependence, so treating these as uncorrelated will artificially lower the χ^2_ν value. If we repeat the LD fit in panel (b) of Fig. 11 neglecting this extra model-dependent uncertainty (i.e. taking the same fractional uncertainty on R_{2N} as we use for a_2), the reduced χ^2_ν value increases from 0.68 to 0.83, as compared to 0.91 for the HV fit. Overall, the LD fit appears to do a better job: the extrapolation of the fit to the deuteron gives essentially zero, as it should, and it has a smaller χ^2 value. However, neither of these differences significantly favors the LD hypothesis.

Next, we remove the intercept as a free parameter (leaving only the slope), and thus constrain the fit by forcing the EMC effect to go through zero for the deuteron ($a_2 = R_{2N} = 1$). The χ^2_ν of this fit should test both the linearity and the consistency with the deuteron, allowing for a more quantitative comparison of the results. For the constrained fit, these can be seen in Fig. 12. The gap in the χ^2 values for the two approaches grows, with 1.17 for HV and 0.61 (0.73 when taking fractional uncertainties from HV case) for LD fits, corresponding to a total change $\Delta\chi^2 = 3.4$ (2.6). While the LD interpretation yields a better description of the data, $\chi^2_\nu = 1.17$ for the HV fit corresponds to a 32% confidence level, so the data are consistent with either hypothesis.

The HV approach with the single parameter fit (HV-0) most closely reflects the previous analysis [26, 33], in that they used a_2 as the measure of SRCs and the raw EMC effect slope. However, the quantitative results of the two analyses differ due to the inclusion of different sets and corrections factors applied to the data. The initial work used the older extractions of a_2 [6] which applied the isoscalar correction that we now know is not appropriate. The correction was applied to all of the experimentally measured $A/^3$He ratios, which were combined with a ^{3}He/^{2}H ratio based largely on a calculation which did not include the isospin correction for ^{3}He. Therefore, even the isoscalar $A/^2$H ratios end up with this correction applied. The authors of Ref. [33] make several independent extractions of the correlation, comparing the EMC results to the original CLAS SRC ratios, as well as the updated JLab Hall C results [9]. They also compare
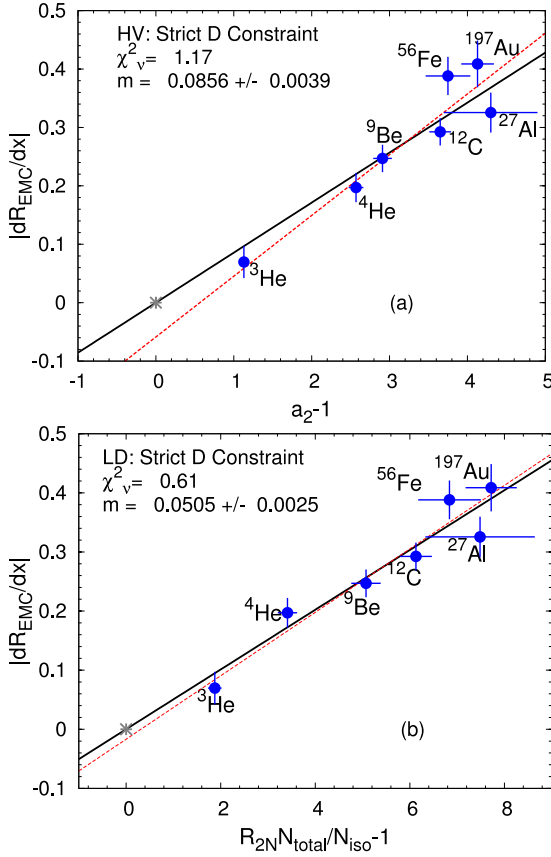
FIG. 12: (color online) EMC slopes vs a_2 (top) and $R_{2N} * N_{tot}/N_{iso}$ (bottom). The solid line is the one-parameter fit, constrained to yield zero for the deuteron (grey point). The dashed red line shows the result of the two-parameter (Fig. 11) for comparison. The fits are almost indistinguishable for the LD tests.

different versions of the Hall C data, using both a_2 and R_{2N}, and also examining a_2 without the coulomb corrections but with the old-style isoscalar corrections, which more closely reflects the analysis of the CLAS data. Note that in the comparison to the Hall C data, they compare the copper SRC ratios to the EMC effect measurements for iron. We use the data shown in Tables I and II for common nuclei only.

While the one-parameter fit is a useful way to compare the relative quality of fits for the LD and HV inspired foundations, it yields an unrealistic estimate for the uncertainties on the fit. Including a deuteron constraint point neglects the fact that there are significant correlated uncertainties in all of the EMC or SRC points from a single experiment, since all of the values are measured relative to the deuteron. Therefore, the statistical and systematic uncertainties in the deuteron data generate an overall normalization of the values for all other nuclei from that measurement which is neglected entirely in this approach. In addition, the linear fit will have extremely small uncertainties for nuclei close to the deuteron, yielding fit uncertainties for light nuclei (or the extrapolation

to the free nucleon) that are significantly smaller than for any existing measurement.

We can evaluate the impact of this and make a more realistic estimate of the fit uncertainties by adding a deuteron constraint point which includes a reasonable estimate of the uncertainty associated with the deuteron measurements in the experiments. We take $|dR_{EMC}/dx| = 0 \pm 0.01$, and $a_2 = R_{2N} = 1 \pm 0.015$, where the error bars were estimated based on deuterium cross section uncertainties from Refs. [32] and [9]. The extracted slope is almost unchanged, while the uncertainty increases by approximately 20%.

TABLE III: Summary of linear fits of EMC effect vs R_{2N} or a_2, and extrapolations to the slopes of the EMC effect for the deuteron, EMC(D), and IMC effect for the deuteron, IMC(D).”-0” denotes a 1-parameter fit, forcing the line to go through zero, corresponding to no EMC effect for the deuteron. “-D” denotes a two parameter fit including a realistic deuteron constraint described in the text. The number in parentheses of the χ^2_ν column includes the result of fitting with smaller fractional errors from a_2.

As Published	χ^2_ν	EMC(D)	IMC(D)
HV (Fig. 11)	0.91	-0.0587 ± 0.037	0.1040 ± 0.012
HV-0 (Fig. 12)	1.17	–	0.0856 ± 0.004
HV-D	1.14	-0.0041 ± 0.010	0.0869 ± 0.005
LD (Fig. 11)	0.68 (0.83)	-0.0168 ± 0.035	0.0537 ± 0.007
LD-0 (Fig. 12)	0.61 (0.73)	–	0.0505 ± 0.003
LD-D	0.60 (0.73)	-0.0013 ± 0.010	0.0508 ± 0.003

The relevant results from the fits are summarized in Table III. As mentioned in the discussion of the EMC effect data, the analyses done for JLab E03013 and SLAC E139 used different isoscalar and Coulomb distortion corrections. We have repeated the above comparisons of the EMC and SRC measurements after estimating the impact of these differences and while the numerical results change slightly (by ≈10% of the uncertainty), they do not affect the trends or the conclusions.

V. POTENTIAL IMPACT OF THE CONNECTION

The close connection between the measurements of the EMC effect and the relative contribution from short-range configurations in nuclei suggests that the modification of the nuclear quark distributions may be related to these short-range structures. However, as seen in the previous section, the connection can be made by both the HV and LD descriptions. Future measurements should allow us to better differentiate between these, but at the moment, we cannot make a definitive conclusion as to the exact nature of this connection. In addition to helping to elucidate the origin of the EMC effect, a better understanding of this correlation will also impact other

attempts to understand nuclear effects based on this relation.

A key aspect of the initial analysis comparing the EMC effect and SRCs [26] was the extrapolation of the EMC effect to the free nucleon, which allows the extraction of the nuclear effects in the deuteron. The authors of Ref. [26] use the fit to extract the IMC (in-medium correction) effect, defined as $\frac{\sigma_A/A}{(\sigma_p+\sigma_n)/2}$, by taking the EMC slope based on the ratio to the deuteron and adding the slope associated with the IMC for the deuteron, $\sigma_d/(\sigma_p+\sigma_n)$, given by the extrapolation of the EMC/SRC linear correlation. Given the IMC for the deuteron, they extract the sum of free proton and neutron structure functions and, subsequently, $F_{2n}(x)$. They obtain an IMC slope for the deuteron of 0.079±0.006 where, as discussed above, the small error is a consequence of using the known values for the deuteron as a constraint while neglecting the correlated uncertainties in the measurements. The equivalent global analysis from their later work, including the new data from Ref. [9], yields 0.084±0.004 [33]. In both cases, they use a fit of the EMC slope as a function of a_2 which is not quite consistent with either our LD (local density) or HV (high virtuality) comparisons.

We repeat this extraction to obtain the IMC slope for the deuteron, using our fits from the previous section and taking the difference of the EMC slope extrapolated to the free nucleon ($a_2 = R_{2N} = 0$) and that for the deuteron. Note that this is equivalent to the intercept parameter, b, of the fits, and taking $dR_{IMC}(D) = b$ accounts for the correlated errors in the EMC slopes for the deuteron and free nucleon. Similarly, one can obtain the IMC slope for $A > 2$ via $dR_{IMC}(A) = dR_{EMC}(A) + dR_{IMC}(D)$.

Our HV fit yields slopes that are close to those from the initial analysis of [26] when we apply a deuteron constraint. The unconstrained linear fit yields a somewhat larger slope, while the LD fits all yield a smaller IMC slope for the deuteron, suggesting smaller nuclear effects. A reanalysis [33] of the deuteron IMC effect with different data sets found its value varied from 0.079 to 0.106, with the largest difference associated with the use of R_{2N} rather than a_2 from the SRC measurements. In the same work, the value for the IMC effect is always larger than our results based on local density picture because they assume that only the high-momentum nucleons associated with the SRCs contribute to the EMC effect, while low-momentum short-distance pairs are included in our local density analysis through the factor N_{tot}/N_{iso}.

The use of the SRC observables to extrapolate measurements of the EMC effect to the free nucleon generates a large range of potential results, with IMC slopes for the deuteron from 0.059 to 0.104, even under the assumption that the correlation is perfectly linear all the way to $A = 2$. In addition, there is still a significant uncertainty associated with the size of the c.m. motion correction, which modifies the extracted values of R_{2N}, changing the IMC slopes for the LD extractions. This range can be significantly narrowed if one can determine whether the underlying connection is related to the density or the vir-

tuality associated with the short-distance configurations. With further studies, this may be possible. If so, the nuclear effects as extrapolated from measurements can be compared with direct calculations of the nuclear effects in the deuteron. A recent study of the model dependence of nuclear effects in the deuteron [75], based on convolution calculations and off-shell effects, produced a range of results for the neutron structure function. For on-shell extractions it is relatively narrow, and a direct comparison to the IMC for the deuteron based on extrapolation from heavier nuclei can provide a constraint on off-shell effects.

However, one must be careful in using this approach to obtain the free neutron structure function, especially at large x values. As discussed in Ref. [75], extrapolations of the EMC effect to the deuteron neglect Fermi motion, which is the dominant effect at $x > 0.6$ and is sensitive to the difference between proton and neutron structure functions at smaller x values. Fermi motion has a significant impact and an important Q^2 dependence in this high-x region [43, 76], neither of which is accounted for in this kind of approach, limiting the reliability of such extrapolations. The off-shell effects as determined from the extrapolation of the EMC effect in Ref. [77] are perfectly consistent with the range of off-shell models included in more recent analyses [75, 78] which examine the model-dependence of the extraction of neutron structure functions, and the large-x deviation between the IMC-based extraction [77] and the results of the microscopic deuteron calculations shown in that work related to the neglect of Fermi motion in the IMC result. Thus, it is necessary to improve our understanding of the connection between the EMC effect and the presence of SRCs, to better constrain the extrapolation, and to explicitly account for both, the effects of Fermi motion and additional nuclear effects, as done in Ref. [36], when going to large x values.

Finally, we note that the connection between the EMC effect and SRCs suggests a mechanism by which the structure function could have an isospin dependence that is not included in most models. In ^{3}He, the singly-occurring neutron is more likely to be at high momentum [11], as the SRCs are dominantly np pairs and the neutron must balance the high-momentum tail of both protons. The neutron also has a larger average local density: the two-body densities from the GFMC calculations [58] show that the two np pairs have a significantly larger contribution for separations below 1 fm than the pp pair. For both the HV and LD explanations of the correlation between SRCs and the EMC effect, this implies a larger EMC effect for the neutron in ^{3}He, and for the proton in ^{3}H.

An isospin dependence in the EMC effect for the $A=3$ nuclei would yield an additional correction to the neutron structure function extracted from DIS on ^{3}He and ^{3}H [79, 80]. It was shown in Ref. [79] that the difference between the nuclear effects in ^{3}He and ^{3}H, defined as $\sigma_A/(Z \times \sigma_p + N \times \sigma_n)$, is extremely small, typically less than 1%

with a spread of ∼1% when varying the nuclear structure, nucleon pdfs, and other aspects of the calculation. Their analysis takes into account the difference between the proton and neutron distributions in the convolution, but not the possibility of isospin dependence in effects beyond the convolution. While it is unlikely to be a very large effect, given the EMC effect for ^{3}He, it may not be a negligible effect in such measurements.

Similarly, the EMC effect in heavy non-isoscalar nuclei may also have a small isospin-dependent component. Such an effect is generally not included in models of the EMC effect, and would have to be accounted for in heavy nuclei or asymmetric nuclear matter [72].

VI.   SUMMARY AND CONCLUSIONS

We examined the A dependence of both the EMC effect and presence of short-range correlations in nuclei and find that the traditional models of a simple density or A dependence fail with the inclusion of the new data on light nuclei. Both observables show similar behavior, suggesting a common origin. We examined the correlation between the two observables under two different assumptions for the underlying physics. In the first, we assume that the EMC effect is driven by the presence of high-momentum nucleons in the nucleus, which is directly extracted in the inclusive measurements at $x > 1$. In the second, we assume that the EMC effect scales with the average local density, and thus correlates with the number of SRCs extracted from the $x > 1$ measurements. We find that under both assumptions, the data are consistent with a linear correlation between the two effects, with the local density comparison yielding a smaller χ^2_ν value.

These results support the local density explanation proposed in Ref. [32], but are still consistent with the explanation in terms of high virtuality [26]. In the end, a more definitive determination of the underlying physics will require further data. A large step in this direction will be taken at JLab after the 12 GeV upgrade. A large set of nuclear targets, including several light nuclei with significant cluster structure, will be used to make high precision measurements of the EMC effect [64] as well as SRCs [81], which will further illuminate the nature of the relationship between the two. The results from these two experiments, combined with heavy target EMC slopes from Jlab E03-103 will more than double the sensitivity of the linear correlation tests.

In addition, measurements probing the modification of nucleon form factors [19, 82] and structure functions [83, 84] as a function of virtuality are planned that will cover a large range of initial momentum, allowing for direct comparison to models of the nuclear effects.

Acknowledgments

[1] W. Czys and K. Gottfried, Ann. Phys. **21**, 47 (1963).
[2] L. L. Frankfurt, M. I. Strikman, D. B. Day, and M. Sargsian, Phys. Rev. C **48**, 2451 (1993).
[3] J. Arrington et al., Phys. Rev. Lett. **82**, 2056 (1999).
[4] J. Arrington et al., Phys. Rev. C **64**, 014602 (2001).
[5] K. S. Egiyan et al., Phys. Rev. C **68**, 014313 (2003).
[6] K. S. Egiyan et al., Phys. Rev. Lett. **96**, 082501 (2006).
[7] R. Shneor et al., Phys. Rev. Lett. **99**, 072501 (2007).
[8] R. Subedi et al., Science **320**, 1476 (2008), 0908.1514.
[9] N. Fomin et al., Phys. Rev. Lett **108**, 092502 (2012).
[10] M. M. Sargsian et al., J. Phys. **G29**, R1 (2003).
[11] J. Arrington, D. Higinbotham, G. Rosner, and M. Sargsian, Prog. Part. Nucl. Phys. **67**, 898 (2012).
[12] A. Antonov and I. Petkov, Il Nuovo Cimento A (1971-1996) **94**, 68 (1986).
[13] M. Lacombe, B. Loiseau, J. M. Richard, R. V. Mau, J. Côté, P. Pirès, and R. de Tourreil, Phys. Rev. C **21**, 861 (1980).
[14] R. B. Wiringa, V. G. J. Stoks, and R. Schiavilla, Phys. Rev. C **51**, 38 (1995).
[15] R. Machleidt, Phys. Rev. C **63**, 024001 (2001).
[16] X. Zhan et al., Phys. Lett. **B705**, 59 (2011).
[17] G. Van Der Steenhoven et al., Phys. Rev. Lett. **57**, 182 (1986).
[18] S. Strauch et al., Phys. Rev. Lett. **91**, 052301 (2003).
[19] M. Paolone, S. Malace, S. Strauch, I. Albayrak, J. Arrington, et al., Phys. Rev. Lett. **105**, 072001 (2010).
[20] I. Sick, Nucl. Phys. **A434**, 677C (1985).
[21] R. D. Mckeown, Phys. Rev. Lett. **56**, 1452 (1986).
[22] J. Jourdan, Nucl. Phys. **A603**, 117 (1996).
[23] J. Morgenstern and Z. Meziani, Phys. Lett. **B515**, 269 (2001).
[24] J. Carlson, J. Jourdan, R. Schiavilla, and I. Sick, Phys. Rev. C **65**, 024002 (2002).
[25] J. Aubert et al., Phys. Lett. **B123**, 275 (1983).
[26] L. Weinstein, E. Piasetzky, D. Higinbotham, J. Gomez, O. Hen, and R. Shneor, Phys. Rev. Lett. **106**, 052301 (2011).
[27] J. Gomez et al., Phys. Rev. D **49**, 4348 (1994).
[28] D. F. Geesaman, K. Saito, and A. W. Thomas, Ann. Rev. Nucl. Sci. **45**, 337 (1995).
[29] P. R. Norton, Rept. Prog. Phys. **66**, 1253 (2003).
[30] F. Gross and S. Liuti, Phys. Rev. C **45**, 1374 (1992).
[31] C. Ciofi degli Atti, L. Frankfurt, L. Kaptari, and

M. Strikman, Phys. Rev. C **76**, 055206 (2007).

[32] J. Seely et al., Phys. Rev. Lett. **103**, 202301 (2009).

[33] O. Hen, E. Piasetzky, and L. Weinstein, Phys. Rev. C **85**, 047301 (2012).

[34] G. Piller and W. Weise, Phys. Rept. **330**, 1 (2000).

[35] C. Ciofi degli Atti and S. Liuti, Phys.Rev. **C44**, 1269 (1991).

[36] S. A. Kulagin and R. Petti, Nucl. Phys. **A765**, 126 (2006).

[37] I. Cloet, W. Bentz, and A. W. Thomas, Phys.Lett. **B642**, 210 (2006).

[38] J. Arrington, R. Ent, C. E. Keppel, J. Mammei, and I. Niculescu, Phys. Rev. C **73**, 035205 (2006).

[39] A. Daniel, Ph.D. thesis (2007).

[40] A. Aste, C. von Arx, and D. Trautmann, Eur. Phys. J. **A26**, 167 (2005).

[41] P. Solvignon, D. Gaskell, and J. Arrington, AIP Conf.Proc. **1160**, 155 (2009).

[42] S. Dasu et al., Phys. Rev. D **49**, 5641 (1994).

[43] J. Arrington, F. Coester, R. Holt, and T.-S. Lee, J. Phys. **G36**, 025005 (2009).

[44] A. Daniel et al., in preparation.

[45] P. Solvignon et al., in preparation.

[46] G. A. Miller and J. R. Smith, Phys. Rev. **C65**, 015211 (2002).

[47] D. S. Koltun, Phys. Rev. C **9**, 484 (1974).

[48] A. E. L. Dieperink and T. d. Forest, Phys. Rev. **C10**, 543 (1974).

[49] R. P. Bickerstaff and W. Thomas, A., J. Phys. **G15** (1989).

[50] G. L. Li, K. F. Liu, and G. E. Brown, Phys. Lett. **B213**, 531 (1988).

[51] S. Kulagin, private communication.

[52] S. A. Kulagin and R. Petti, Phys. Rev. C **82**, 054614 (2010).

[53] O. Benhar and I. Sick (2012), arXiv:1207.4595.

[54] G. Brown, M. Buballa, Z. B. Li, and J. Wambach, Nucl.Phys. **A593**, 295 (1995).

[55] O. Benhar, V. R. Pandharipande, and I. Sick, Phys. Lett. **B410**, 79 (1997).

[56] O. Benhar, A. Fabrocini, and S. Fantoni, Nucl. Phys. **A505**, 267 (1989).

[57] I. Sick and D. Day, Phys. Lett. **B274**, 16 (1992).

[58] S. C. Pieper and R. B. Wiringa, Ann. Rev. Nucl. Part. Sci. **51**, 53 (2001).

[59] S. Pieper, private communication.

[60] H. De Vries, C. W. De Jager, and C. De Vries, Atom. Data Nucl. Data Tabl. **36**, 495 (1987).

[61] K. Arai, Y. Ogawa, Y. Suzuki, and K. Varga, Phys. Rev. C **54**, 132 (1996).

[62] M. Hirai, S. Kumano, K. Saito, and T. Watanabe, Phys. Rev. C **83**, 035202 (2011).

[63] S. Pandit, V. Jha, K. Mahata, S. Santra, C. Palshetkar, et al., Phys. Rev. C **84**, 031601 (2011).

[64] J. Arrington, A. Daniel, and D. Gaskell, Jefferson Lab experiment E12-10-008.

[65] O. Benhar, D. Day, and I. Sick, Rev. Mod. Phys. **80**, 189 (2008).

[66] C. C. degli Atti et al., Phys. Rev. C **44**, R7 (1991).

[67] C. C. degli Atti and S. Simula, Phys. Rev. C **53**, 1689 (1996).

[68] E. Piasetzky, M. Sargsian, L. Frankfurt, M. Strikman, and J. Watson, Phys. Rev. Lett. **97**, 162504 (2006).

[69] M. M. Sargsian, T. V. Abrahamyan, M. I. Strikman, and L. L. Frankfurt, Phys. Rev. C **71**, 044615 (2005).

[70] R. Schiavilla, R. B. Wiringa, S. C. Pieper, and J. Carlson, Phys. Rev. Lett. **98**, 132501 (2007).

[71] M. Vanhalst, J. Ryckebusch, and W. Cosyn, Phys.Rev. **C86**, 044619 (2012).

[72] M. McGauley and M. M. Sargsian (2011), arXiv:1102.3973.

[73] M. Vanhalst, W. Cosyn, and J. Ryckebusch, Phys.Rev. **C84**, 031302 (2011).

[74] M. Sato, S. Coon, H. Pirner, and J. Vary, Phys.Rev. **C33**, 1062 (1986).

[75] J. Arrington, J. Rubin, and W. Melnitchouk, Phys. Rev. Lett. **108**, 252001 (2012).

[76] A. Accardi, M. Christy, C. Keppel, P. Monaghan, W. Melnitchouk, J. Morfin, and J. Owens, Phys. Rev. D **81**, 034016 (2010).

[77] O. Hen, A. Accardi, W. Melnitchouk, and E. Piasetzky, Phys. Rev. D **84**, 117501 (2011).

[78] A. Accardi, W. Melnitchouk, J. Owens, M. Christy, C. Keppel, et al., Phys.Rev. **D84**, 014008 (2011).

[79] I. R. Afnan et al., Phys. Rev. C **68**, 035201 (2003).

[80] G. G. Petratos, J. Gomez, R. J. Holt, and R. D. Ransom, Jefferson Lab experiment E12-10-103.

[81] J. Arrington, D. Day, N. Fomin, and P. Solvignon, Jefferson Lab experiment E12-06-105.

[82] E. Brash, G. M. Huber, R. Ransome, and S. Strauch, Jefferson Lab experiment E12-11-002.

[83] A. V. Klimenko et al., Phys. Rev. C **73**, 035212 (2006).

[84] O. Hen, L. B. Weinstein, S. Gilad, and S. A. Wood, Jefferson Lab experiment E12-11-107.